machines
MDPI
Article

A Smart Tool Holder Calibrated by Machine Learning for Measuring Cutting Force in Fine Turning and Its Application to the Specific Cutting Force of Low Carbon Steel S15C

Liang-Wei Tseng, Teng-Shan Hu and Yuh-Chung Hu *

Department of Mechanical and Electromechanical Engineering, National ILan University, Yilan 26047, Taiwan; B0722096@ms.niu.edu.tw (L.-W.T.); B0722076@ms.niu.edu.tw (T.-S.H.)
* Correspondence: ychu@niu.edu.tw; Tel.: +886-3-9317469

Abstract: Real-time monitoring of the cutting force in the machining process is critical for improving machining accuracy, optimizing the machining process, and optimizing tool lifetime; however, the dynamometers are too expensive to be widely used by machine tool users. Therefore, this paper presents a simple and cheap apparatus—a smart tool holder—to measure the cutting force of turning tools in the finishing turning. The apparatus does not change the structure of the turning tool. It consists of a tool holder and a piezoresistive force sensor foil, and transmits the signal through Bluetooth wireless communication. Instead of dealing with the circuit hardware, this paper uses the Artificial Neural Network (ANN) model to successfully calibrate the warm-up shift problem of the piezoresistive force sensor. Such a software method is simple, and considerably cheaper than the hardware method. For the force measurement capability of the smart tool holder, the cross-interference between orthogonal forces are very small and thus can be ignored. The force reading of the smart tool holder possesses high repeatability for the same turning parameters and high accuracy within the experiment groups. The authors apply the smart tool holder to cut the low carbon steel S15C, and to determine its specific cutting force in fine turning. The resulting fine turning force model agrees very well with the measurement. Its mean absolute deviation is 3.87% and its standard deviation is 1.55%, which reveals that the accuracy and precision of the smart tool holder and the fine turning force model are both good.

Keywords: CNC lathe; cutting force; dynamometer; intelligent machine; machine learning; machine tool; neural network; piezoresistive force sensor; turning tool holder; warm-up shift calibration

check for updates

Citation: Tseng, L.-W.; Hu, T.-S.; Hu, Y.-C. A Smart Tool Holder Calibrated by Machine Learning for Measuring Cutting Force in Fine Turning and Its Application to the Specific Cutting Force of Low Carbon Steel S15C. *Machines* **2021**, *9*, 190. https://doi.org/10.3390/machines9090190

Academic Editor: Kai Cheng

Received: 2 August 2021
Accepted: 4 September 2021
Published: 6 September 2021

1. Introduction

If the machine tool can monitor the cutting force in the machining process, then it could detect and prevent chatter early in order to ensure the required surface roughness, to ensure the dimensional stability while needless of a downstream workpiece measurement, and to analyze the machining process and optimize the run and tool lifetime. The products related to the cutting force measurement are the spike® sensor system produced by pro-micron GmbH [1], and the dynamometer produced by Kistler GmbH [2]. However, such products are too expensive to be widely used in the production lines of machine tool users.

Based on the mechanics of materials, when a mechanical structure is subject to forces/stress, the mechanical structure will be deformed/strained. Theoretically, one can deduce the cutting force from the strain of the cutting tool; however, this is not feasible, because to maintain the machining accuracy, the cutting tool must be very rigid, so its strain is too small to detect. Therefore, two mechanisms are necessary for measuring the cutting force. One is to amplify the strain to be detectable, namely through a transmission structure that can transmit the cutting force and amplify the strain; and the other is to convert the mechanical strain into electrical signals (voltage or current), namely through a transducer. However, there is a trade-off between the rigidity of the force transmission structure and the sensitivity of the transducer to the cutting force, because the strain amplification increases the sensitivity of the transducer while also reducing the rigidity of the cutting tool. The literature related to the cutting force measurement aimed to solve the trade-off problem mentioned above. The designs of the force transmission structures are varied, and there are three common types of force transducers: piezoresistive force sensors, capacitive force sensors, and piezoelectric force sensors.

Zhao et al. [3] bonded four MEMS strain gauges onto the four bonding slots on the surfaces of the turning tool shank. In this case, the signal cables were connected to the outside through the signal cable channel that penetrates the turning tool shank. Their design could measure both the tangential and radial components of the cutting force simultaneously. Süleyman et al. [4] designed a piezoresistive dynamometer composed of four octagonal ring structures bonded with strain gauges to measure the three components (tangential, radial, and axial) of the cutting force, namely the cutting force, the passive force, and the feed force. Zhao et al. [5] designed a turning tool holder with two mutual perpendicular octagonal ring structures bonded with semi-conductive strain gauges to measure the three components of the cutting force. In order to increase the sensitivity of the force sensing, Zhang et al. [6] designed a turning tool shank with an elastomer and eight strain film sensors. The elastomer is a cubic structure with four stepped grooves inside of it, and it is between two parallel octagonal connection plates. Both ends of the strain film sensors are bonded on the edges of the two parallel octagonal connection plates. Li et al. [7] embedded a Ni-Cr strain film sensor on the surface of the turning tool shank by screw, and connected the signal cables to the outside through the signal cable channel that penetrates the turning tool shank. Rizal et al. [8] developed a 3-axis dynamometer based on strain gauge for the cutting force measurement in turning. Their force transmission structure is composed of four octagonal ring structures and 16 strain gauges, which were bolted between two plates (top and bottom plates). The bottom plate was used to install the dynamometer on the lathe turret, and the turning tool was installed on the top plate; however, its sensitivity was very small, with only tens of μV/N. Pham et al. [9] pasted four optical strain gauges onto the four surfaces of the turning tool shank to measure the triaxial cutting force components in turning. Its operation principle was Fiber Bragg Grating (FBG). Its sensitivity was very small, with only tens to hundreds of pm/N. Therefore, the signal processing at the rear end was a challenge. Uquillas and Yeh [10] drilled four cavities onto the four sides of the turning tool shank, and each cavity was attached with a strain gauge to measure the cutting force; however, such a design seems unacceptable to the tool manufacturers because it destroys the original design of the tool shank, especially in regard to the rigidity. Gong et al. [11] embedded a piezoresistive ceramic (SiAlCO) directly under the insert to measure the cutting force in turning; however, its measurable range was only within about 10 N.

Kim et al. [12] installed a cylindrical capacitive displacement sensor around the spindle to measure the displacement of the spindle, and estimated the cutting force of the milling tool from the displacement of the spindle. Xie et al. [13] refitted a standard milling tool holder to have deformable beams. The deformable beams transmit the cutting force and amplify the strain. The deformation of the deformable beams make the changes of the gaps between them and the fixed electrodes. As a result, one can deduce the cutting force from the capacitance changes.

Wang et al. [14] installed a piezoelectric film (PZT) strain sensor directly under the insert of the turning tool to measure the cutting force. Chen et al. [15] refitted the turning tool into two parts, where the upper part was the tool shank and the other was the base part. A piezoelectric film sensor was bolted between the upper and base parts to measure the cutting force. The upper part was cut with a slot and another piezoelectric film sensor was bolted in the slot to measure the feed force; however, the measurable range of the force was only within 10 N. Xiao et al. [16] drilled two shallow cavities on the top and the bottom side of the turning tool shank near the insert, and attached a PZT film sensor in each cavity to measure the cutting force; however, the measurable range of the force was only within 10 N. Nguyen et al. [17] pasted piezoelectric film (PVDF) strain sensors on the surface of the cutting tool shank to measure the cutting force. Capacitive force sensors have the advantages of a high sensitivity and an immunity to the external environment, but their disadvantages are that they are highly nonlinear and susceptible to parasitic capacitance. Piezoelectric force sensors have the advantages of a high sensitivity and signal-to-noise ratio, but their disadvantages are that they have a bad current response, they are not resistant to a humid environment, and they are un-sensitive to static response. Piezoresistive pressures have the advantages of a high sensitivity and output voltage and a low cost, but their disadvantage is that they are very sensitive to temperature change.

In summary, the cutting force measurement apparatus requires a transmission structure that can transmit the cutting force and amplify the strain, and a transducer to convert the mechanical strain into an electrical signal. In order to meet the users' requirement for the machining accuracy of machine tools and for the cutting force measurement, here are two design considerations:

1. The transmission structure has to be flexible enough to be sensitive to the cutting force, but it cannot be too flexible and thereby reduce the machining accuracy;
2. The transducer has to be low cost, and must be able to withstand the dirty and humid machining environment.

Therefore, this paper presents a simple and cheap apparatus to measure the tangential component of the cutting force of the turning tool. The apparatus does not change the structure of the turning tool. It consists of a tool holder and a piezoresistive film sensor and transmit the signal through Bluetooth wireless transmission. The whole apparatus is packaged in a metal shielding, so it can withstand the dirty and humid machining environment.

2. Materials and Methods

2.1. The Cutting Force Model of Longitudinal Turning

The force action between the turning tool and the workpiece can be sectioned into three components: the major cutting force (F_c), the feed force (F_f), and the passive force (F_p) (Figure 1). The factors affecting the cutting force include the workpiece material, the cutting speed, the feed rate, the depth of cut, the tool geometry, the tool material, and the tool wear. Based on Kienzle model of the cutting force in longitudinal turning [18,19], the cutting force (F_c) is equal to the product of the specific cutting force (k_c) and the sectional area of chip (A), namely:

$$F_c = k_c \cdot A, \tag{1}$$

where the sectional area of the chip is equal to the product of the cut thickness (h) and the cut width (b). F_c is in Newton, k_c is in N/mm^2, and h and b are in mm. Furthermore, h and b are dependent on the feed rate (f) and the depth of cut (a_p), namely:

$$h = f \cdot \sin\kappa,\ b = a_p / \sin\kappa, \tag{2}$$

where κ is the tool cutting edge angle and f and a_p are in mm/rev and mm, respectively. Therefore, the cutting force formula can be expressed as:

$$F_c = k_c \cdot f \cdot a_p. \tag{3}$$

Since the cutting force is dependent on the aforesaid factors affecting the cutting force, the specific cutting force (k_c) is determined through many correction coefficients relating to the workpiece material, the tool geometry and property, and the machining parameters, which is given by:

$$k_c = k_{c1,1} \cdot h^{-z} \cdot K_\gamma \cdot K_v \cdot K_{st} \cdot K_{ver}, \quad (4)$$

where, K_γ, K_v, K_{st}, and K_{ver} are, respectively, the correction coefficients for the rake angle (γ), the cutting speed (v) in m/min, the chip compression, and the tool wear. Moreover, z is the material constant, $k_{c1,1}$ is the basic cutting force for the specific workpiece material, which is related to h = 1 mm, b = 1 mm, κ = 45°, v = 100 m/min, γ = +6°, and the tool material is cemented carbide. The values of $k_{c1,1}$ and z are regarded as workpiece material constants, which are taken from the material tables. The values of other correction coefficients are given by:

$$\begin{gathered} K_\gamma = 1 - \tfrac{\gamma-\gamma_0}{100},\ \gamma_0 = +6^\circ \text{ for cutting steel,} \\ K_v = 1.03 - \tfrac{3v}{10^4}, \\ K_{st} = 1.0 \text{ for longitudinal turning,} \end{gathered} \quad (5)$$

and the value of K_{ver} is 1.3 to 1.5, in general, which relates the rise of the force of a dulling tool to that of the sharp tool and its value.

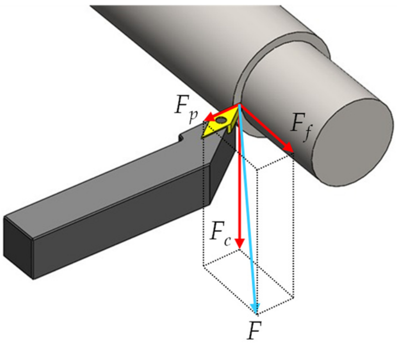

Figure 1. The schematic diagram of the cutting force in longitudinal turning.

This paper aims to develop a smart tool holder with a force sensing capability, and will demonstrate its capability of measuring the cutting force (F_c) in the longitudinal turning of low carbon steel. The cutting force measured by the smart tool holder will be compared with the values calculated by the Kienzle model.

The turning tool manufacturing industry has been developed for more than two centuries, and the turning tool structure has been standardized. Changing the structure of the turning tool will change its rigidity, and thereby may reduce its usage lifetime and machining accuracy. Changing the structure of the turning tool is unacceptable in the industry. Therefore, this paper aims to develop an external smart tool holder embedded with a piezoresistive film sensor to measure the cutting force. The method does not change the structure of the turning tool, nor does it change the clamping method of the tool turret. The following subsections will describe the smart tool holder design and manufacture, as well as the piezoresistive force sensor and its assembly in detail.

2.2. The Design and Manufacture of Smart Tool Holder

This paper uses Tongtai TS-85 bedroom CNC lathe to demonstrate the proposed smart tool holder. The smart tool holder is designed for the standard turning tool, model SVJCR-2525M16 (Figure 2a), and it is adaptive to the tool turret of the demonstrated CNC lathe (Figure 2b). The turning tool is clamped onto the tool turret through a wedge structure (Figure 2c). Table 1 details the specifications of the model SVJCR-2525M16 turning tool.

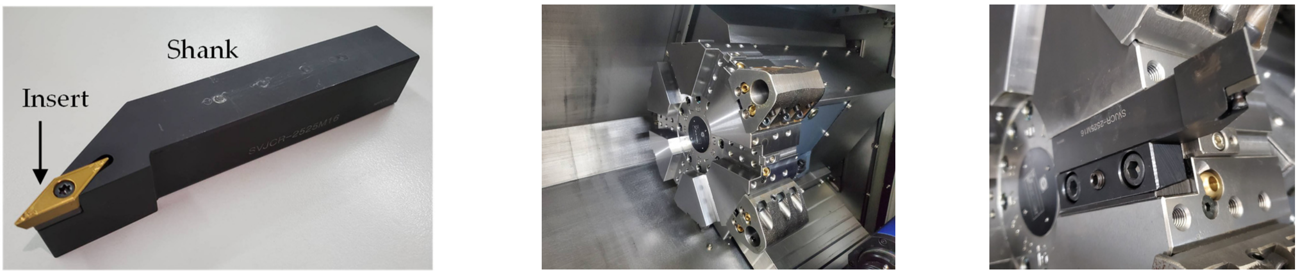

(**a**) (**b**) (**c**)

Figure 2. The proposed smart tool holder is designed for: (**a**) the standard turning tool, model: SVJCR-2525M16; (**b**) the tool turret of the Tongtai TS-85 CNC bedroom lathe; and (**c**) the turning tool clamped on the tool turret.

Table 1. The specification of the model SVJCR-2525M16 turning tool and the model VCMT160404HQ insert.

Model SVJCR-2525M16 turning tool							
Order No.	H	B	LF	LH	WF	Cutting-edge angle (κ)	Rake angle (γ)
SVJCR-2525M16	25 mm	25 mm	150 mm	38 mm	32 mm	93°	0°

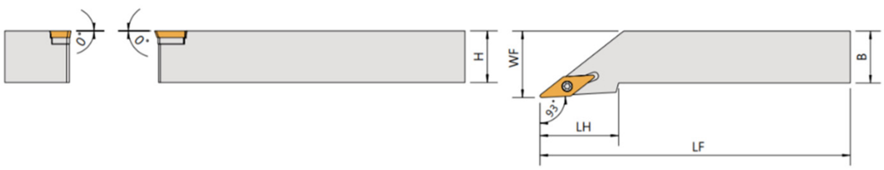

Model VCMT160404HQ insert			
Style: VMCT Grade: CA525 Inscribe circle (IC): 9.53 mm Relief angle: 7° Material: Carbide Coating composition: TiCn/Al_2O_3/TiN Primary workpiece: Steel Usage classification: Light interruption	Size: 331 Thickness (S): 4.76 mm Hole diameter (D1): 4.4 mm Include angle: 35° Material grade: Micro columnar Shape: Diamond	Chipbreaker: HQ Corner radius (RE): 0.4 mm Rake: Positive Number of cutting edges: 2 Coating process: CVD Insert hand: Neutral Insert holding method: Screw Cutting range: Finishing medium	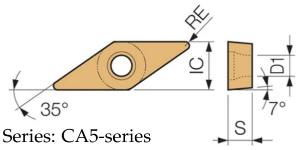 Series: CA5-series
Application: External turning, copying, facing, undercutting, profiling, internal facing, back boring.			

The smart tool holder consists of five parts (Figure 3a), wherein parts 1 and 2 are, respectively, the front and rear covers and are used to clamp the tool, and parts 3 to 5 construct the wedge structure for installing the smart tool holder on the lathe turret. The wedge structure is assembled through two M6 hexagon socket screws, and an M6 set screw is used to adjust its height in order to ensure that the smart tool holder is firmly installed on the lathe turret. Ten M6 hexagon socket screws (Figure 3b) assemble parts 1 and 2. Four M6 set screws (Figure 3c) adjust the clamping tightness of the turning tool.

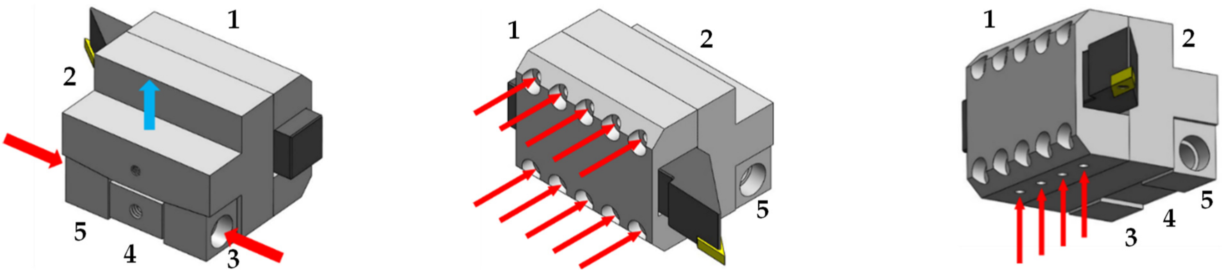

(**a**) (**b**) (**c**)

Figure 3. The structure of the smart tool holder consists of: (**a**) the five parts of the smart tool holder, including the front cover (part 1), the rear cover (part 2), and the wedge, composed of parts 3 to 5; (**b**) parts 1 and 2, which are assembled by ten M6 hexagon socket screws; and (**c**) the clamping tightness of the turning tool, which is adjusted by four M6 set screws.

The authors determine the material for the smart tool holder based on the Kienzle model of the cutting force and the finite element simulation. For cutting low carbon steel, JIS S15C (Table 2), in the cut depth range of 0.1 to 0.3 mm and the feed rate range of 0.1 to 0.2 mm/rev, the maximum theoretical value of the cutting force is about 165 N (Table 3). Applying a cutting force of 250 N—about 1.5 times the maximum theoretical value—on the cutting edge of the insert, the result of the finite element simulation (Figure 4) shows that the maximum stress is about 12.92 N/mm^2. Therefore, the yielding strength of the structure of the smart tool holder must be greater than 12.92 MPa. Based on the simulation results and the literature [20], the authors select the medium carbon steel, S45C, as the material of the smart tool holder. S45C is a common structural material due to the advantages of wear resistance, high strength and toughness, and good machining properties. Figure 5 shows the completed structure of the smart tool holder. It is composed of five parts. Parts 1 and 2 are the front and rear covers, respectively. Parts 3 to 5 form a wedge through which the smart tool holder is installed on the turret.

Table 2. The material and geometrical properties of the low carbon steel JIS S15C workpiece.

Composition in wt%	**C**	**Mn**	**P**	**S**	**Si**
	0.13–0.18	0.3–0.6	≤0.03	≤0.035	0.15–0.35
Material property	**Yield strength**	**Tensile strength**	**Elongation**	**Hardness HB**	
	≥235 N/mm^2	≥370 N/mm^2	≥30%	111–167 (Normal)	111–149 (Anneal)
Geometrical property	**Geometry**		**Length**	**Diameter**	
	Rod		200 mm	60 mm	

Table 3. The parameters related to the cutting force calculation through Kienzle model.

Material parameters, JIS S15C	Basic specific cutting force, $k_{c1,1}$ (N/mm^2)		Material constant, z					
	1820 [18]		0.22					
Tool parameters	Rake angle, γ		Cutting edge angle, κ					
	0°		93°					
Constant machining parameters	Spindle speed (rpm)		Cutting speed (m/min)					
	500		94.25					
Correction coefficients	K_γ	K_v	K_{st}			K_{ver}		
	1.06	1.00	1.00			1.00		
Variable machining parameters	Depth of cut, a_p (mm)		0.1			0.3		
	Feed rate, f (mm/rev)		0.10	0.15	0.20	0.10	0.15	0.20
Specific cutting force, k_c (N/mm^2), calculated by Equation (4)			3202	2929	2749	3202	2929	2749
Cutting force, F_c (N)			32.02	43.93	54.98	96.06	131.80	164.94

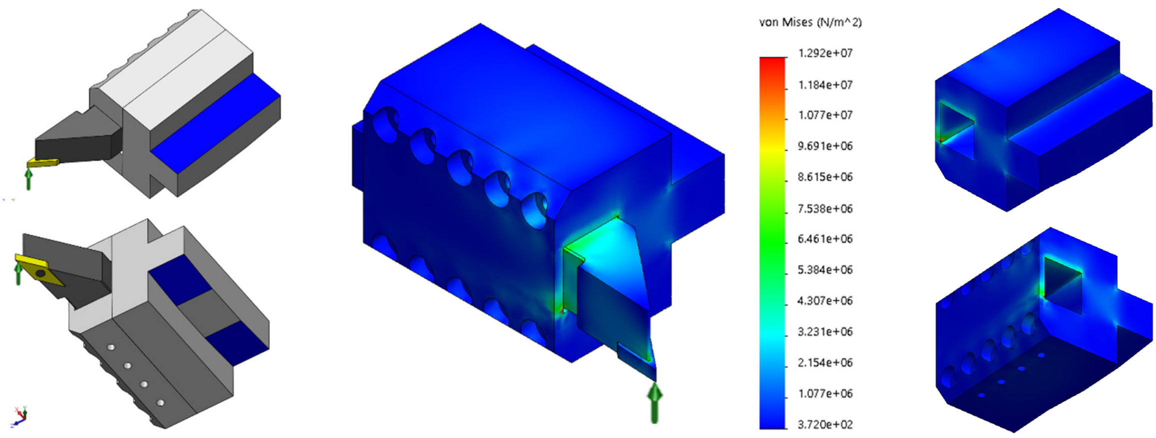

(a) (b) (c)

Figure 4. The stress field of the smart tool holder subject to the cutting force based on finite element simulation: (**a**) the fixed boundaries being shown on the blue surfaces; (**b**) the stress field of the combination of the turning tool and the smart tool holder; and (**c**) the backside and front-side views of the stress field of the smart tool holder.

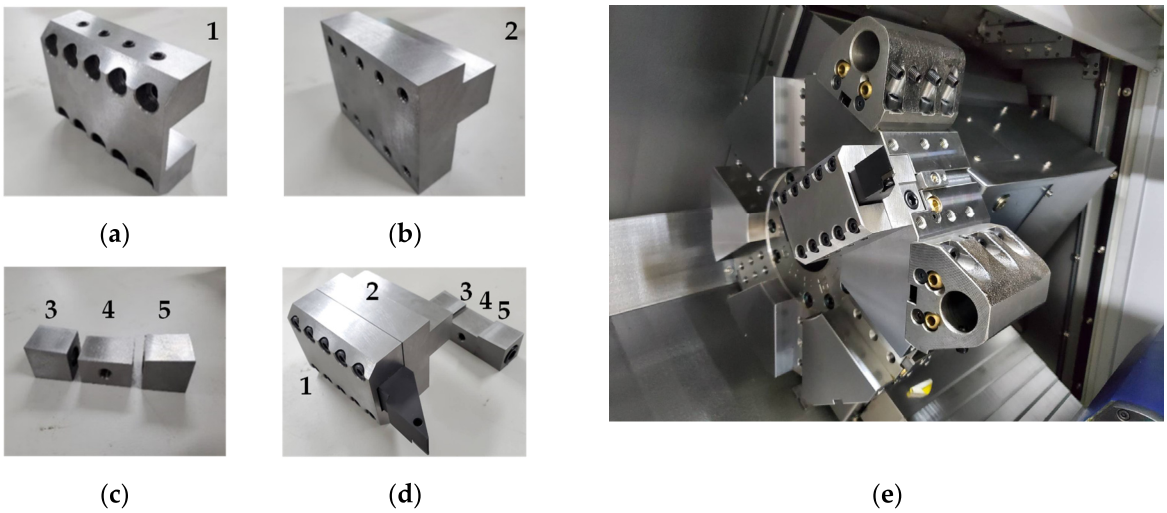

Figure 5. The completed structure of the smart tool holder: (**a**) Part 1 is the front cover; (**b**) part 2 is the rear cover; (**c**) parts 3 to 5 form the wedge through which the smart tool holder is installed on the turret; (**d**) the smart tool holder clamping the turning tool; and (**e**) the assembly of the smart tool holder and turning tool installed on the turret through the wedge.

2.3. Force Sensor Device and Assembly

In addition to the structure of the smart tool holder, it requires a transducer that can convert the mechanical strain into electrical signal, namely the force sensor. The following subsections will describe the force sensor device and its assembly with the tool holder structure.

2.3.1. Force Sensor Device

Since the transducer has to be embedded in the gap between the smart tool holder and the turning tool, the authors select a metal film force sensor, model GIS-S-1-C10, which is produced by G-Chen Technology Corp., Taiwan. It is a piezoresistive force sensor with a built-in Wheatstone bridge circuit and is packaged into the flexible PET foil (Figure 6a). Furthermore, it is resistant to vibration and impact, thereby suitable for the machining environment of the CNC lathe. The force sensor device consists of the film force sensor and the data acquisition toolbox. The data acquisition toolbox transmits data to the personal computer next to the machine tool through Bluetooth (Figure 6b). Table 4 lists the specification of the force sensor device.

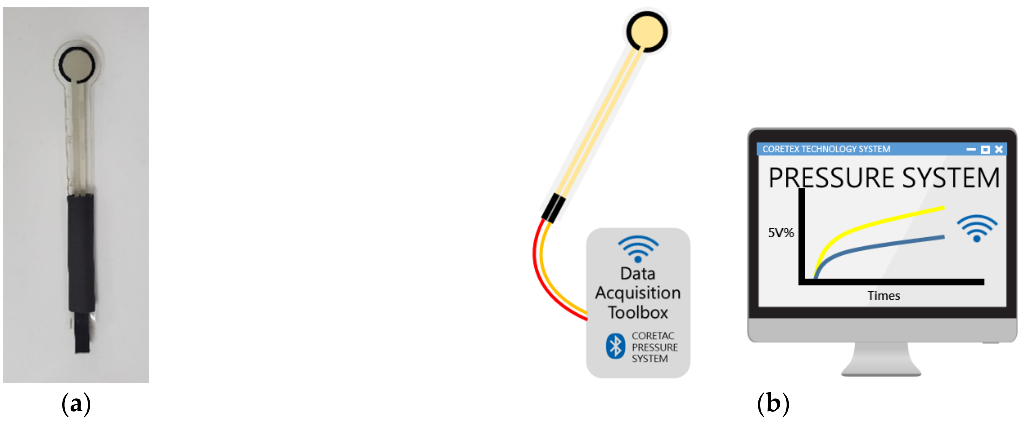

Figure 6. The force sensor device: (**a**) the flexible force sensor foil, and (**b**) the schematic diagram of the flexible force sensor foil connecting to a data acquisition toolbox. The data acquisition toolbox transmits data to the personal computer next to the machine tool through Bluetooth.

Table 4. The specification of the force sensor device.

Item	Value
Diameter of sensing area	10 mm
Maximum sensing area	78.5 mm^2
PET foil thickness	0.25 mm
Maximum sensing force	245 N
Minimum sensing dimension	0.5 mm × 0.5 mm
Power supply	Type +5V, Type 5 mA (max.)
Linearity	<±3%
Repeatability	<±2.5% Full sensing range
Hysteresis	<±4.5% Full sensing range
Drift	<5% Logarithmic time scale
Response time	<5 µs
Sampling rate	100 Hz

2.3.2. The Assembly of Smart Tool Holder

The film force sensor is to be clamped between the bottom surface of the turning tool and part 1 (Figure 5a) of the smart tool holder, as shown in Figure 7a. If the film force sensor is directly clamped between the bottom surface of the turning tool and part 1 of the smart tool holder, the clamping force may exceed the maximum sensing force of the film force sensor. Therefore, the authors insert a metal gasket between the bottom surface of the turning tool and part 1 of the smart tool holder. By adjusting four M6 set screws of part 1 of the smart tool holder and the position of the metal gasket (Figure 3c), one can ensure that the clamping force applied to the film force sensor will not exceed its maximum sensing force and, furthermore, can firmly clamp the turning tool. The film force sensor should be bonded between the bottom surface of the turning tool to avoid issues. Part 1 of the smart tool holder is best for determining the sensitivity of the force measurement. Next, consider the assembly of the turning tool, the smart tool holder, and the metal shim, like Figure 4b; analyze the stress distribution at the bottom surface of the turning tool along its longitudinal axis (Figure 7a) when the assembly is subjected to the cutting forces of 9.81 N (1 kgw) and 78.48 N (8 kgw), respectively. Figure 7b shows the result of the finite element simulation, wherein two stress peaks occur at the two edges of the metal gasket. Subtracting the stress distribution of 1 kgw from that of 8 kgw (Figure 7c) reveals that the position nearest to the insert is most sensitive to the change of the cutting force. Thus, the bonding position of the film force sensor is determined (Figure 7d). Figure 8 shows the completed smart tool holder that is clamping a turning tool. The smart tool holder includes the tool holder structure, the film force sensor, and the wireless data acquisition unit. Four M6 set screws numbered as 1 to 4 in Figure 8 control the pre-stress of the film force sensor.

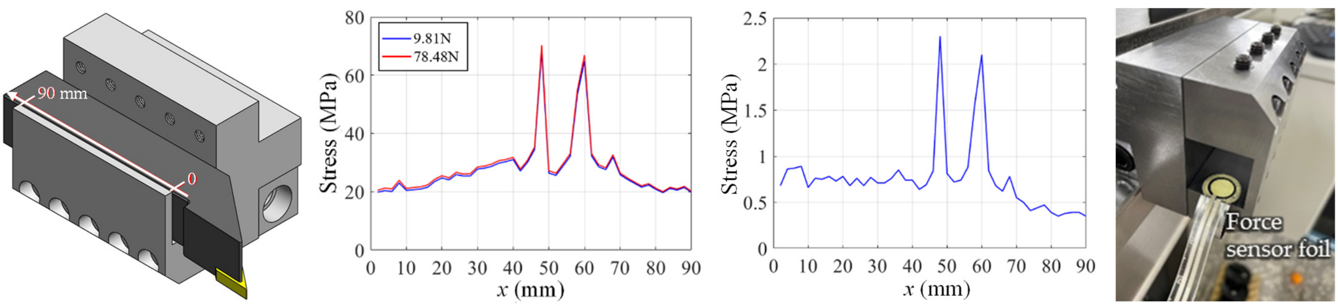

(**a**) (**b**) (**c**) (**d**)

Figure 7. The determination process of the position of the film force sensor: (**a**) the schematic diagram of the longitudinal coordinate of the turning tool; (**b**) the stress distribution at the bottom surface of the turning tool along its longitudinal axis when subject to cutting force; (**c**) the stress difference of (**b**); (**d**) the bonding position of the film force sensor.

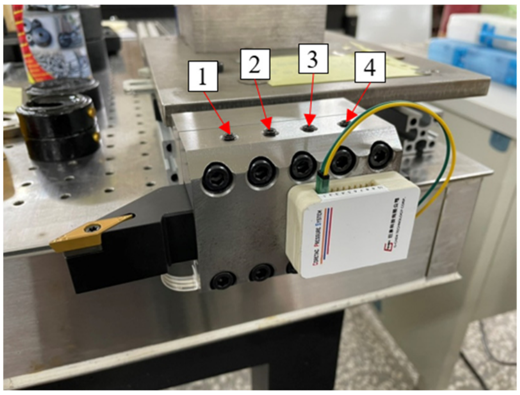

Figure 8. The completed smart tool holder that is clamping a turning tool. The smart tool holder includes the tool holder structure, the film force sensor, and the wireless data acquisition unit.

3. Results

The following subsections will describe the test of the smart tool holder detail, which includes the static test and the dynamic test. The static test includes the calibration through the Neural Network model and the test of the cross-interference of the cutting force components. The dynamic test is the turning test on the demonstration machine tool that is the bedroom CNC lathe of model TS-85 manufactured by Tongtai Machine and Tool Co., Ltd (Kaohsiung, Taiwan).

3.1. Static Test

The static test is used to test the response of the smart tool holder to static load, calibrate the force measurement, and check the cross-interference of the cutting force components. The cutting force can be sectioned into three components (Figure 9a): the main cutting force (F_c), the feed force (F_f), and the passive force (F_p). In order to simulate the situation on the turret, the authors make a fixture to clamp the assembly of the turning tool and the smart tool holder on an optical table (Figure 9b). The smart tool holder is used to measure the main cutting force; therefore, the authors apply the main cutting force on the cutting edge of the turning tool through hanging standard weights (Figure 9b). The masses of the standard weights are 100 g, 200 g, 500 g, 1000 g, and 2000 g. The wireless data acquisition unit of the smart tool holder transmits the data to the personal computer via Bluetooth.

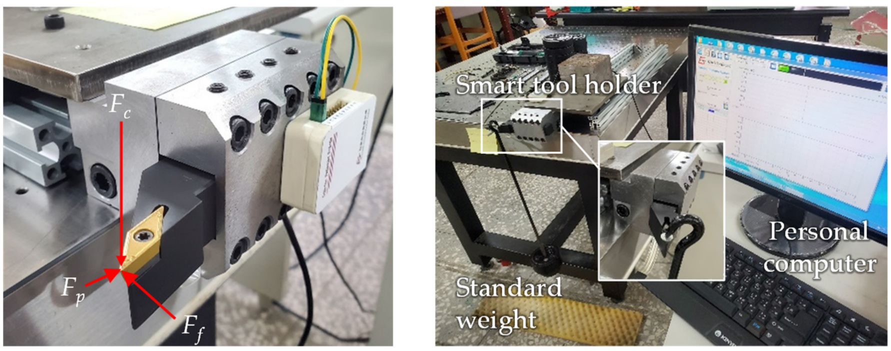

(**a**) (**b**)

Figure 9. The static load test of the smart tool holder: (**a**) the turning tool and smart tool holder clamped on the optical table in order to simulate their installation on the turret; and (**b**) the experiment setup of the static load test.

3.1.1. Static Load Test

In order to ensure the condition is the same for each test, the assembly of the turning tool and the smart tool holder is tightened by a torque wrench in constant torque. In addition, by tightening the four set screws (Figure 8) in constant torque, the pre-stress of the film force sensor is the same for each test. Figure 10 shows the output signal of the film force sensor in terms of voltage under variety constant cutting force. Theoretically, the output signal should be constant when subject to constant force; however, unfortunately, the output signal will shift with time. This is the warm-up shift phenomenon in force sensors [21]. Such a shift is unacceptable in devices requiring accuracy at all times. The primary two sources of the warm-up shift in force sensors are the warm-up shift of the sensing element, and that related to the system's temperature compensation technique. The present smart tool holder does not have temperature compensation; therefore, the signal shift phenomenon should come from the warm-up shift of the sensing element. This is due to the unbalance of the Wheatstone bridge caused by the surface temperature and resultant hot spots on the sensor foil when the temperature of the sensing element rises. To solve this problem, one can reduce the actuation voltage to reduce the temperature rise of the sensing element and, consequently, reduce the warm-up shift phenomenon; however, reducing the actuation voltage also reduces the signal level of the sensor and, consequently, adversely affects the noise level. Another solution is reducing the duty-cycle of the power supply to the sensor. This is more sophisticated, but does not affect the noise level. Instead of the previously mentioned two solutions, the authors will try to adopt machine learning to calibrate the warm-up shift of the signal in the following sub-subsection.

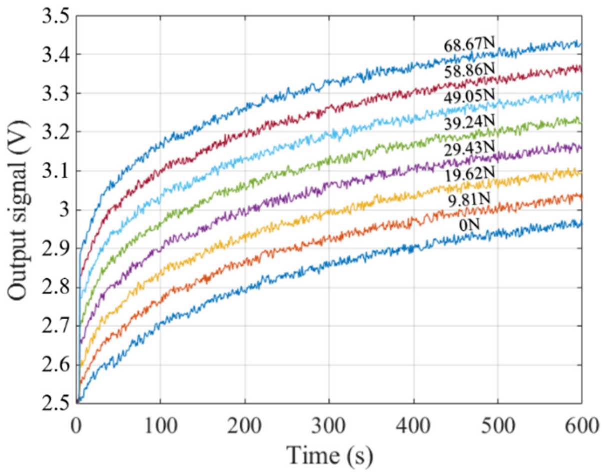

Figure 10. The output signal of the film force sensor under variety cutting force magnitudes.

3.1.2. The Calibration of Warm-up Shift through Artificial Neural Network

Artificial Neural Network (ANN), one model of the machine learning, is a simplified model that mimics the way that the human brain processes information. It is used to correlate the input data set and the output data set through the adjustment of the weighting numbers and activation function of neurons. The adjustment is based on the learning rule. ANN consists of many neurons. A neuron (Figure 11a) is composed of weighted numbers, bias, and an activation function. The output of a neuron, y, is expressed as

$$y = f\left(\sum_{i=1}^{n} (x_i w_{ij}) + b_i\right) = f(\mathbf{X}\mathbf{W}_j^T + b_j), \tag{6}$$

wherein $\mathbf{X}$ is the input vector whose elements are the input data set, $\{x_1, x_2, x_3, \ldots, x_n\}$, ${\mathbf{W}_j}^T$ is the transpose of the weighting vector, $\mathbf{W}_j$, of the j-th layer whose elements are the weighted numbers, $\{w_{1j}, w_{2j}, w_{3j}, \ldots, w_{nj}\}$, b_j is the initial state of the neuron called bias, and $f(x)$ is the activation function. The neuron multiplies each input data with a weighted number and then calculates their summation. Then, it transforms the summation added with a bias into an output through the activation function. ANN is composed of an input layer, an output layer, and single or multiple hidden layers (Figure 11b). Each hidden layer may contain many neurons, and the input/output layer could be single or multiple input/output. The output of a neuron will be the input of the neuron in the next layer.

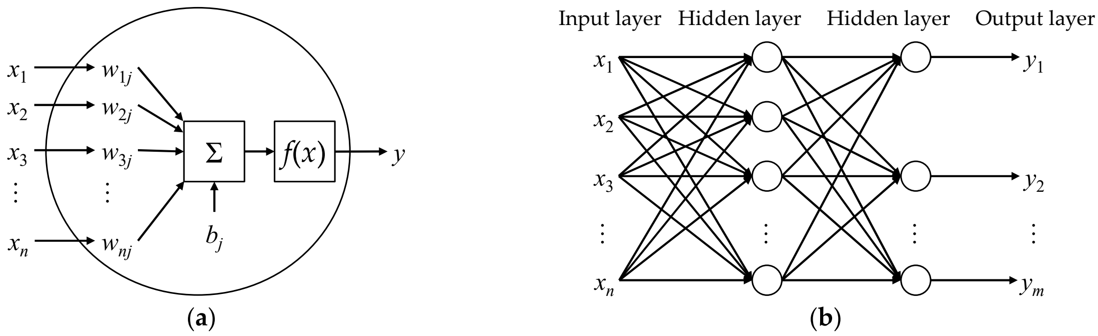

Figure 11. The schematic diagram of Artificial Neural Network: (**a**) a neuron; and (**b**) the artificial neural network.

In order to calibrate the warm-up shift of the output signal of the smart tool holder, the authors use an ANN with a single hidden layer. The input of the ANN model is the time series of the output voltages of the force sensor, and the output is the applied loads. The experiment shown in Figure 9 under the load of 0 to 15 kgw (147.15 N) to collect the data at the sampling rate of 50 Hz is repeated, wherein 80% of the data serves as the training data and the remaining 20% as the testing data. There are 480,000 training data samples in the model training. The training data is used to train the ANN model, and the testing data is used to test the performance of the resulting model. The input data set of ANN is the time-series of the output signal of the smart tool holder when subject to a specific load within 10 min. The input data includes the output signal of the film force sensor and the time, and the output data set is the load. The activation function is hyperbolic tangent function, defined as:

$$f(x) = \frac{e^x - e^{-x}}{e^x + e^{-x}}, \tag{7}$$

which will transform the data into the value between -1 and +1 (Figure 12). The training process is to reduce the error between the prediction of the ANN model and the output of the training data set gradually through modifying the weighted numbers. The authors use Mean Square Error (MSE) as the index for judging the accuracy of the ANN model, which is defined as:

$$\text{MSE} = \frac{1}{m}\sum_{i=1}^{m}(y_i - \hat{y}_i)^2, \tag{8}$$

where $\hat{y}_i$ is the prediction of the ANN model. Therefore, the problem becomes an optimization problem, namely to minimize the MSE.

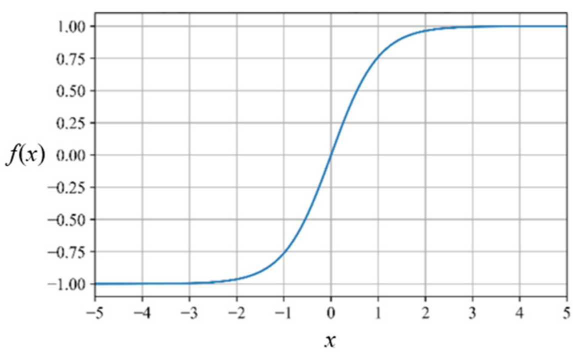

Figure 12. The hyperbolic tangent function.

The authors adopt the function “Neural Net Fitting” in the App of “Machine Learning and Deep Learning” built in MATLAB to build the ANN model, and adopt the Levenberg-Marquardt algorithm to solve the minimization problem of the MSE. The learning curve (Figure 13) shows that the ANN model converges very soon, and that the minimum MSE approach is 0.04 after 40 epochs, which means the accuracy of the ANN model reaches 99.9%.

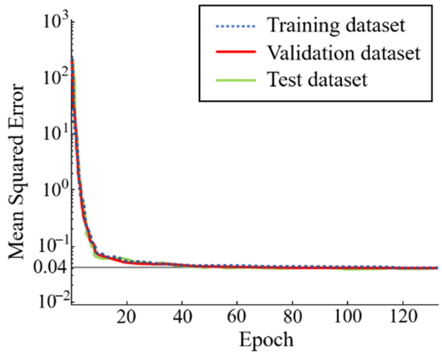

Figure 13. The learning curve of the ANN model.

Finally, the authors collect other data sets to validate the ANN model. The validation data sets must never participate in the training process, and the validation process is called external validation. The external validation data set is the output signal of the film force sensor when it is subjected to a changing load within 6 min. The load changing process is

1. Zero load lasts 1 min.;
2. Add on 2-kgw (19.62 N) standard weight and then remove it after 1 min.;
3. Add on 2-kgw (19.62 N) standard weight again and then remove it after 1 min.;
4. Add on 3-kgw (29.43 N) standard weight and then remove it after 1 min.;
5. Add on 1-kgw (9.81 N) standard weight and then remove it after 1 min.

Figure 14a shows the raw data of the external validation set. Figure 14b shows the readings of the smart tool holder with ANN calibration. The warm-up shift phenomenon disappeared.

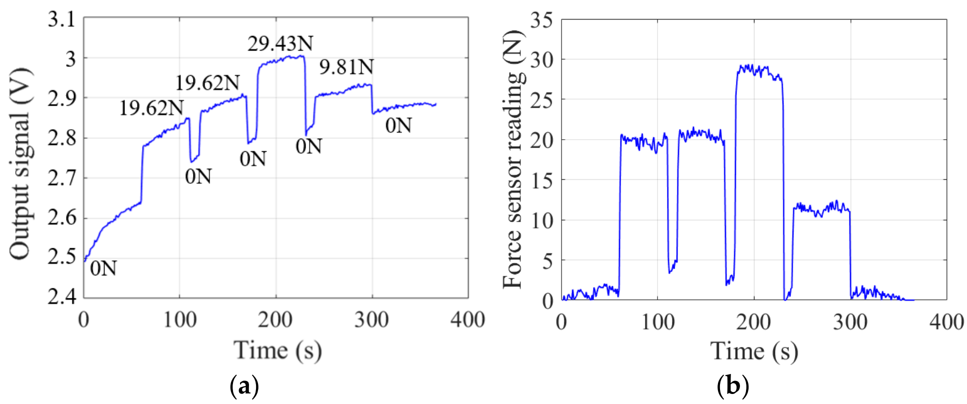

Figure 14. The external validation of the ANN model: (**a**) the raw data of the external validation set; and (**b**) the force sensor reading of the smart tool holder with ANN calibration.

3.1.3. The Cross-Interference Test

This paper aims to measure major cutting force (F_c) (Figure 1); however, the feed force (F_f) and the passive force (F_p) may interfere with the measurement of the major cutting force (F_c), namely the cross-interference. Therefore, the authors use standard weights to apply feed and passive forces to the turning tool, respectively. They then test whether the feed and passive force will interfere with the force sensor reading of the smart tool holder.

The standard weights are 1 kg (9.81 N), 2 kg (19.62 N), 3 kg (29.43 N), 4 kg (39.24 N), 5 kg (49.05 N), 6 kg (58.86 N), 7 kg (68.67 N), 8 kg (78.48 N), 9 kg (88.29 N), 10 kg (98.10 N), 11 kg (107.91 N), and 12 kg (117.72 N). Table 5 lists the results of the cross-interference test. The mean cross-interference of the feed force (F_f) and the passive force (F_p) with the major cutting force (F_c) are only 1.44% and 1.75%, respectively.

Table 5. The results of the cross-interference test.

F_f (N)	9.81	19.62	29.43	39.24	49.05	58.86	68.67	78.48	88.29	98.10	107.91	117.72
Force sensor reading (N)	0.00	0.00	0.00	0.00	0.21	3.68	2.38	1.93	0.79	0.96	2.12	0.99
XI% *	0.00	0.00	0.00	0.00	0.43	6.25	3.47	2.46	0.89	0.98	1.96	0.84
MXI% *	1.44											
F_p (N)	9.81	19.62	29.43	39.24	49.05	58.86	68.67	78.48	88.29	98.10	107.91	117.72
Force sensor reading (N)	0.60	0.20	0.00	0.00	0.51	0.87	0.91	1.32	1.65	2.16	2.37	2.41
XI%	6.12	1.02	0.00	0.00	1.04	1.48	1.33	1.68	1.87	2.20	2.20	2.05
MXI%	1.75											

* *XI*%: Cross-interference percentage, where *XI*% = (*Reading*/F_f)·100% or (*Reading*/F_p)·100%; *MXI*%: Mean cross-interference percentage, where *MXI*% = the mean value of *XI*%.

Finally, the authors apply the cutting forces (F_c) to the smart tool holder through adding the standard weights gradually, and record its readings (Table 6). The results show the mean error is 2.77% when the cutting force is within 12 kgw (117.72 N), and the greater the cutting force, the smaller the measurement error.

Table 6. The error test of the major cutting force measurement.

F_c (N)	9.81	19.62	29.43	39.24	49.05	58.86	68.67	78.48	88.29	98.10	107.91	117.72
Force sensor reading (N)	11.06	21.01	31.09	40.40	49.42	59.07	68.51	78.59	89.73	97.45	106.79	117.66
E% *	12.74	7.08	5.64	2.96	0.75	0.36	0.23	0.14	1.63	0.66	1.04	0.05
ME% *	2.77											

* *E*%: Measurement error percentage, where *E*% = ($|Reading - F_c| / F_c$)·100%; *ME*%: Mean measurement error percentage, where *ME*% = the mean value of *E*%.

3.2. Turning Test

After completing the smart tool holder, the authors proceed to the turning experiment. The turning experiment will conduct a constant and variable feed rate, respectively, under a different depth of cut. The turning experiment is used to test whether the smart tool holder is robust enough to withstand the machining environment, as well as its response to the cutting force. The following sub-subsections will describe the experiment setup and the results in detail.

3.2.1. Experiment Setup

The turning experiment is conducted on the Tongtai TS-85 bedroom CNC lathe produced by Tongtai Machine and Tool Co., Ltd. in Taiwan (Figure 15a). Figure 15b shows the workpiece and the combination of the turning tool and the smart tool holder installed on the machine tool. The output signal of the smart tool holder is transferred to the personal computer next to the machine tool through Bluetooth wireless communication. Figure 15c,d, respectively, show the smart tool holder with and without metal protective shielding, respectively, installed on the machine tool. The workpiece is a low carbon steel S15C rod with a length of 200 mm and a diameter of 60 mm. Since the suspended length of the workpiece is only 150 mm, it does not need to set up the tail stock during the cutting process. The turning experiment shows that the rigidity of the smart tool holder is robust enough to withstand the machining environment; however, the splashing of the hot chips will interfere with the output signal and damage the flexible circuit board of the film force sensor. Therefore, the authors cover the smart tool holder with aluminum protective shielding (Figure 15d). The machining parameters will be described in the following sub-subsection in detail.

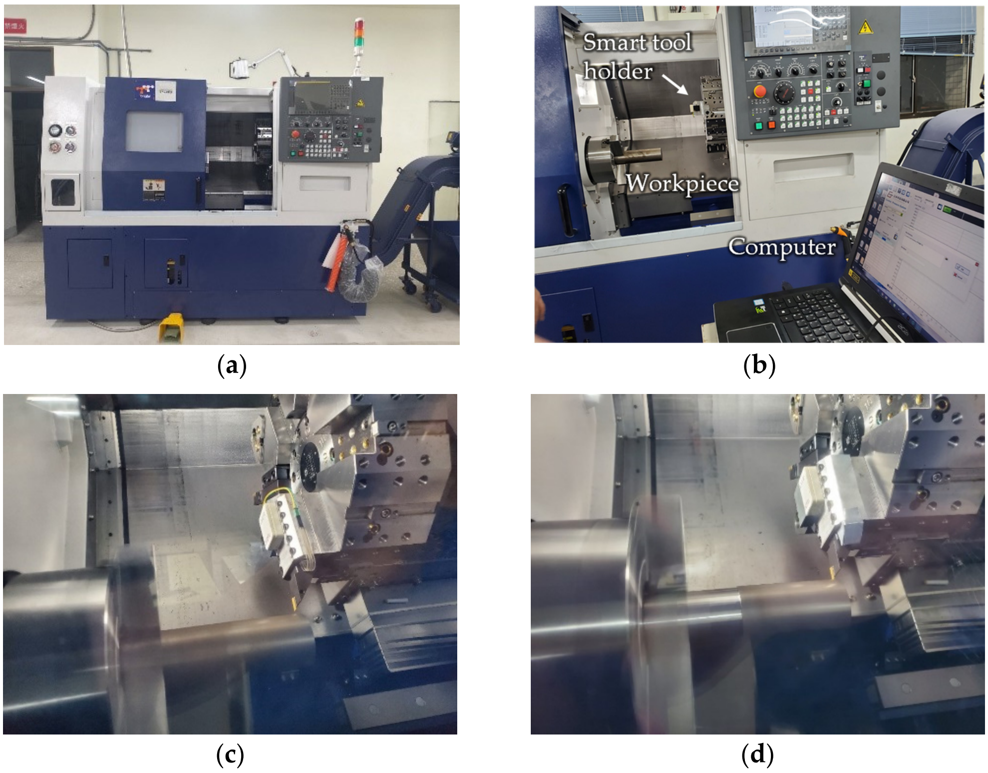

Figure 15. The turning experiment setup: (**a**) Tongtai TS-85 bedroom CNC lathe; (**b**) the workpiece, smart tool holder, and the turning tool installed on the machine tool, and a personal computer next the machine tool; (**c**) the bare smart tool holder; and (**d**) the smart tool holder with aluminum protective shielding.

3.2.2. Turning Test

The turning test conducts the outer diameter turning of a low carbon steel S15C rod with a 60-mm diameter (Figure 16). The spindle rotates at the speed of 500 rpm. There are two working conditions for the turning experiment. One is at a constant depth of cut (a_p) and feed rate (f) and the other is at a constant a_p, but a variable f.

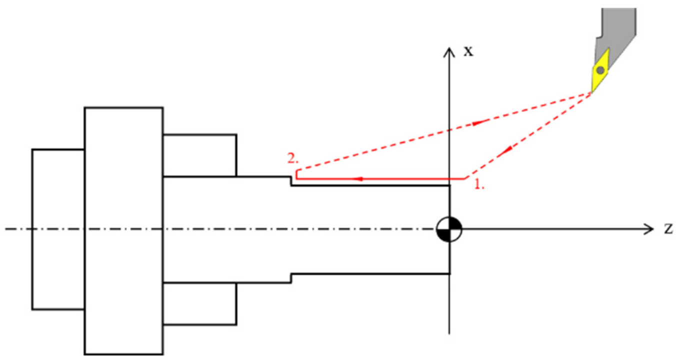

Figure 16. The schematic diagram of outer diameter turning.

For the working condition of the constant depth of cut and feed rate, the cutting length is 90 mm, and a_p and f are 0.1 mm and 0.1 mm/rev, 0.3 mm and 0.1 mm/rev, 0.1 mm and 0.2 mm/rev, and 0.3 mm and 0.2 mm/rev, respectively. Figure 17 shows the force sensor readings of the smart tool holder when turning at a constant feed rate and depth of cut, which reveals that, at a constant feed rate, the force sensor reading of a_p = 0.3 mm is about three times that of a_p = 0.1 mm, and, at a constant depth of cut, the reading of f = 0.2 mm/rev is about 1.7 times that of f = 0.1 mm. This trend agrees with the Kienzle model.

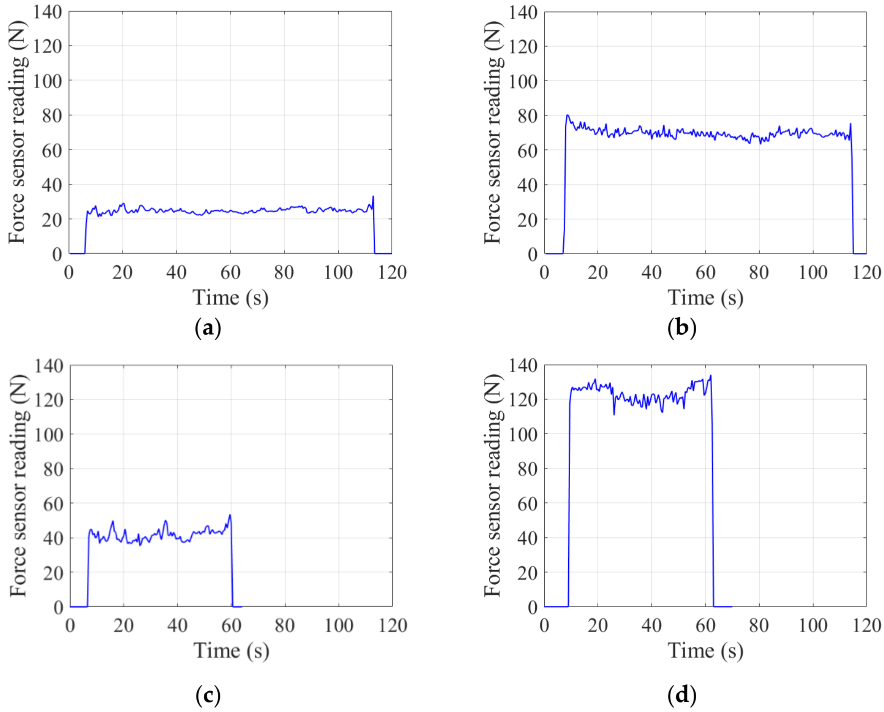

Figure 17. The force sensor readings of the smart tool holder at the working condition of constant feed rate (f) and cutting depth (ap): (**a**) f = 0.1 mm/rev, ap = 0.1 mm; (**b**) f = 0.1 mm/rev, ap = 0.3; (**c**) f = 0.2 mm/rev, a_p = 0.1 mm; and (**d**) f = 0.2 mm/rev, a_p = 0.3 mm. The spindle rotates at 500 rpm and the cut length is 90 mm.

For the working condition of the variable feed rate, a_p is constant, the cutting length is 90 mm, and f is changed every 30 mm in the order of 0.1 mm/rev, 0.15 mm/rev, and 0.2 mm/rev. Figure 18 shows the force sensor readings of the smart tool holder when turning at a variable feed rate, which reveals that the response of the smart tool holder is fast enough to catch the change of the feed rate. Furthermore, the force sensor readings are consistent with those of the working conditions of the constant feed rate (Figure 17).

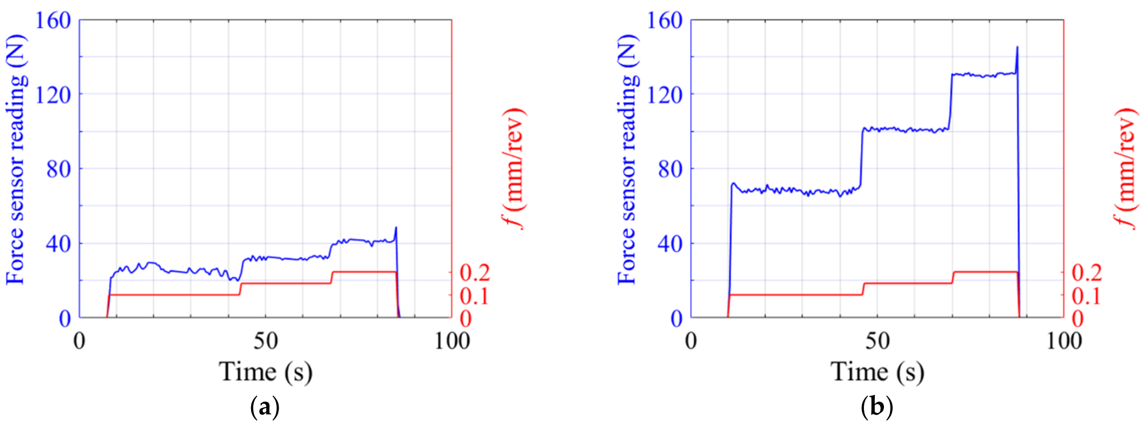

Figure 18. The force sensor readings of the smart tool holder at the working condition of varying feed rate (f). The cutting length is 90 mm, f is changed every 30 mm in the order of 0.1 mm/rev, 0.15 mm/rev, and 0.2 mm/rev, and the constant cutting depth is, respectively, (**a**) ap = 0.1 mm; and (**b**) ap = 0.3 mm. The spindle rotates at 500 rpm.

3.2.3. Comparison with the Theoretical Model of Cutting Theory

Table 7 lists the comparison of the force sensor readings of the smart tool holder (F_c') in the above turning test, and the theoretical values (F_c) calculated by the Kienzle model, namely with Equation (3). The force sensor readings of the smart tool holder are smaller than the theoretical values. The mean absolute deviation is 24.77% and the standard deviation (σ) of the absolute deviations is 3.05%. The absolute deviations are within 1σ. Figure 19 shows the variation of the ratio of the cutting force to the depth of cut (F_c/a_p) with respect to the feed rate (f). Based on the Kienzle model, the variation of F_c/a_p with respect to f is linear, and that of the force sensor readings of the smart tool holder is also linear. In summary, based on Table 7 and Figure 19, the precision of the cutting force measurement of the smart tool holder is very good, but its accuracy is slightly worse; however, the accuracy problem can be solved by adding a shift value to the force sensor readings of the smart tool holder. The trend of the force sensor readings of the smart tool holder agrees with the Kienzle model [22,23].

Table 7. The comparison of the readings of the smart tool holder with the theoretical values.

a_p (mm)	f (mm/rev)	k_c (N/mm^2)	F_c(N)	F_c/a_p (N/mm)	F_c'(N)	F_c'/a_p (N/mm)	∣Deviation∣%
0.1	0.1	3202	32.02	320.2	24.92	249.2	22.17
	0.15	2929	43.93	439.3	31.98	319.8	27.21
	0.2	2749	54.98	549.8	40.91	409.1	25.59
0.3	0.1	3202	96.06	320.2	68.18	227.3	29.02
	0.15	2929	131.80	439.3	100.75	335.8	23.56
	0.2	2749	164.94	549.8	130.18	433.9	21.07
					Mean deviation		24.77
					Standard deviation, σ		3.05

F_c is calculated by the Kienzle model, namely with Equation (3); F_c' is measured by the smart tool holder; Deviation% = $\frac{|F_c' - F_c|}{F_c} \times 100\%$.

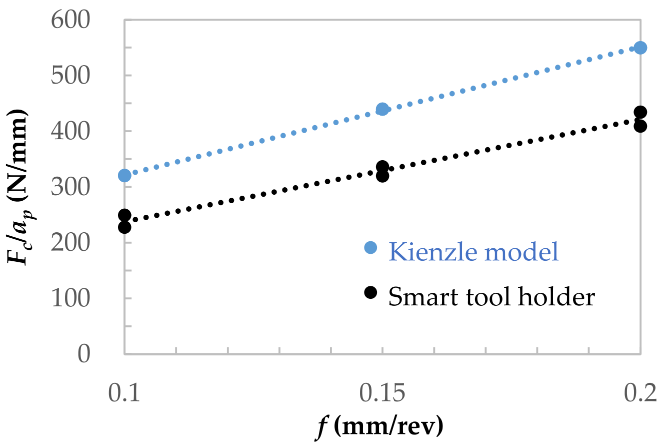

Figure 19. The variation of the ratio of the cutting force (F_c) to the depth of cut (a_p) with respect to the feed rate (f).

4. Discussion

Instead of dealing with the circuit hardware, this paper adopts a software strategy which uses the ANN model to calibrate the warm-up shift problem of the piezoresistive force sensor. It turns out that the ANN model successfully eliminates the warm-up shift of the piezoresistive force sensor (Figure 14). The software method is simple and considerably cheaper than the hardware method. For the force measurement capability of the present smart tool holder, the cross-interference between orthogonal forces (Table 5) are very small and can be ignored, and the mean error of its static force measurement is within 3% (Table 6). The force reading of the smart tool holder possesses high precision within the experiment groups (Table 7) because the standard deviation (σ) of the absolute deviations is only 3.05% and the deviations of all experiments are within 1σ. However, the accuracy is not very good. Fortunately, the force sensor readings of the smart tool holder are lower than the theoretical values by about 24.77% on average, and the variation of the readings of each experiment is within 1σ, namely 3.05%.

The above comparison is based on the Kienzle model. However, the Kienzle model is applicable to the range of rough turning, namely, the depth of cut (a_p) is considerably larger than the nose radius of the insert (r_e). Referring to Tables 1, 3 and 7, the nose radius of insert is 0.4 mm, while the depth of cut is only between 0.1 to 0.3 mm. Therefore, the Kienzle model has to be modified to be applicable to finishing turning. Horváth [24] had proposed a model for fine turning forces. He introduced the equivalent cut thickness (h_{eq}) and cut width (b_{eq}) to describe the chip geometry in fine turning, and modified the Kienzle model. The equivalent cut thickness and cut width are defined as:

$$b_{\mathrm{eq}} = \frac{a_p - r_e(1-\cos\kappa)}{\sin\kappa} + r_e\left(\kappa + \sin^{-1}\frac{f}{2r_e}\right), \text{ and } h_{\mathrm{eq}} = \frac{a_p \cdot f}{b_{\mathrm{eq}}}, \tag{9}$$

Then $A = b \cdot h = a_p \cdot f = b_{\mathrm{eq}} \cdot h_{\mathrm{eq}}$, and

$$k_c = \frac{F_c}{A} = \frac{F_c}{b_{\mathrm{eq}} \cdot h_{\mathrm{eq}}}. \tag{10}$$

Since the specific cutting force is dependent on b_{eq} and h_{eq}, then, based on the Kienzle model, one can assume that:

$$k_c = C \cdot b_{\mathrm{eq}}^{-y} \cdot h_{\mathrm{eq}}^{-z}. \tag{11}$$

Since the depth of cut, a_p, in fine turning is usually smaller than 0.5 mm, which results in $h_{\mathrm{eq}} < 1$ mm, then the basic specific cutting force, $k_{c1,1}$, in the Kienzle model can no longer be applicable to fine turning. Horváth [24] proposed a basic specific cutting force, $k_{c1,0.1}$, referring to $b_{\mathrm{eq}} = 1$ mm and $h_{\mathrm{eq}} = 0.1$ mm. Substituting $b_{\mathrm{eq}} = 1$ mm and $h_{\mathrm{eq}} = 0.1$ mm into Equations (10) and (11) yields:

$$k_{c1,0.1} = C \cdot 0.1^{-z}, \tag{12}$$

$$k_c = k_{c1,0.1} \cdot 10^{-z} \cdot b_{\mathrm{eq}}^{-y} \cdot h_{\mathrm{eq}}^{-z}, \tag{13}$$

$$F_c = k_{c1,0.1} \cdot 10^{-z} \cdot b_{\mathrm{eq}}^{1-y} \cdot h_{\mathrm{eq}}^{1-z}. \tag{14}$$

Taking the logarithm of Equation (13) yields:

$$\log(k_c) = \log(k_{c1,0.1}) - z - y \cdot \log(b_{\mathrm{eq}}) - z \cdot \log(h_{\mathrm{eq}}), \tag{15}$$

which reveals that the relationship between $\log(k_c)$, $\log(b_{\mathrm{eq}})$, and $\log(h_{\mathrm{eq}})$ is linear. With the values given in the columns 7 to 9 in Table 8, one can obtain the values of $k_{c1,0.1}$, z, and y by linear regression,

$$k_{c1,0.1} = 2571, \ z = 0.2724, \text{ and } y = -0.4689. \tag{16}$$

Consequently, the formulas of the specific cutting force and cutting force for the fine turning of low carbon steel S15C are given:

$$k_c = 2571 \cdot 10^{-0.2724} \cdot b_{\mathrm{eff}}^{0.4689} \cdot h_{\mathrm{eq}}^{-0.2724}, \tag{17}$$

$$F_c = k_c \cdot b_{\mathrm{eff}} \cdot h_{\mathrm{eq}} = 2571 \cdot 10^{-0.2724} \cdot b_{\mathrm{eff}}^{1.4689} \cdot h_{\mathrm{eq}}^{0.7276}. \tag{18}$$

The last second column of Table 8 lists the cutting forces calculated by Equation (18). The last column of Table 8 lists the absolute deviation percentages between the cutting forces measured by the smart tool holder and those calculated by the fine turning model of Equation (18). Their mean value is 3.87% and standard deviation is 1.55%, which reveals that both the accuracy and the precision of the smart tool holder are both good. Figure 20 visualizes the consistency of the measured and calculated cutting force values in the fine turning of low carbon steel S15C.

Table 8. The fine turning parameters of low carbon steel S15C and the cutting forces, wherein the nose radius of insert (r_e) is 0.4 mm, the cutting edge angle (κ) is 1.6232 rad (93°).

a_p (mm)	f (mm)	$F_c{}'$ (N) [1]	b_{eq} (mm) [2]	h_{eq} (mm) [3]	k_c (N/mm^2) [4]	log(b_{eq})	log(h_{eq})	log(k_c)	F_c (N) [5]	∣Force Deviation∣% [6]
0.1	0.1	24.92	0.3780	0.0265	2492	−0.4225	−1.5775	3.3965	23.41	6.47
0.1	0.15	31.98	0.4033	0.0372	2132	−0.3943	−1.4296	3.3288	32.98	3.04
0.1	0.2	40.91	0.4290	0.0466	2046	−0.3676	−1.3314	3.3108	42.56	3.89
0.3	0.1	68.18	0.5783	0.0519	2273	−0.2379	−1.2850	3.3565	71.34	4.43
0.3	0.15	100.75	0.6036	0.0746	2239	−0.2192	−1.1275	3.3500	98.91	1.86
0.3	0.2	130.18	0.6292	0.0954	2170	−0.2012	−1.0207	3.3364	125.76	3.51
Mean value of ∣Force deviation∣%										3.87
Standard deviation of ∣Force deviation∣%										1.55

[1] The cutting force measured by the smart tool holder; [2] the equivalent cut width calculated by Equation (9); [3] the equivalent cut thickness calculated by Equation (9); [4] the specific cutting force calculated by $F_c{}'/(b_{eq} \cdot h_{eq})$; [5] the cutting force calculated by Equation (18); [6] ∣Forced deviation∣% = $\frac{|F_c' - F_c|}{F_c} \cdot 100\%$.

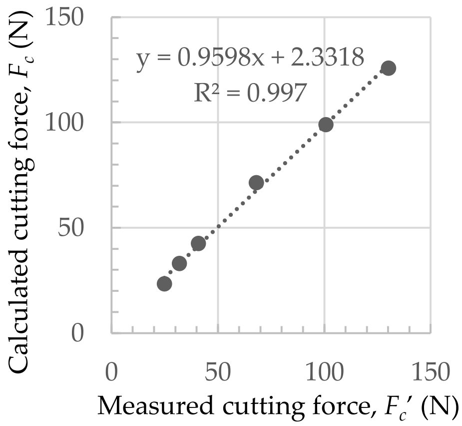

Figure 20. The comparison of measured and calculated cutting force in the fine turning of low carbon steel S15C.

5. Conclusions

The smart tool holder can successfully read the cutting force in the turning process, and withstands the machining environment; however, the usage of four M6 set screws to adjust the pre-stress of the force sensor foil is still inconvenient. Therefore, there is still room for improvement in its structure design. Instead of dealing with the circuit hardware, this paper adopts software strategy, namely the machine learning (ANN model), to successfully solve the problem of the warm-up shift of the force sensor. This will dramatically reduce the cost of the force sensors. In addition, the authors apply the smart tool holder to cut the low carbon steel S15C, and to determine the specific cutting force of the low carbon steel S15C for fine turning. The resulting fine turning force model agrees very well with the measurement.

Author Contributions: Conceptualization, Y.-C.H.; methodology, L.-W.T. and T.-S.H.; software, L.-W.T. and T.-S.H.; validation, L.-W.T. and T.-S.H.; formal analysis, Y.-C.H.; investigation, L.-W.T. and T.-S.H.; resources, Y.-C.H.; data curation, L.-W.T. and T.-S.H.; writing—original draft preparation, L.-W.T., T.-S.H., and Y.-C.H.; writing—review and editing, Y.-C.H.; visualization, L.-W.T. and T.-S.H.; supervision, Y.-C.H.; project administration, Y.-C.H.; funding acquisition, Y.-C.H. All authors have read and agreed to the published version of the manuscript.

Funding: This research was funded by the Ministry of Science and Technology, Taiwan, grant number MOST 110-2221-E-197-029, MOST 110-2622-E-197-009.

Institutional Review Board Statement: Not applicable.

Informed Consent Statement: Not applicable.

Data Availability Statement: Not applicable.

Conflicts of Interest: The authors declare no conflict of interest. The funders had no role in the design of the study; in the collection, analyses, or interpretation of data; in the writing of the manuscript; or in the decision to publish the results.

References

1. Pro-Micron GmbH. Available online: https://www.pro-micron.de/?lang=en (accessed on 17 July 2021).
2. Kistler GmbH, Data Sheet of 3-Component Measuring System for Cutting Force Measurement during Turning, Type 9129A. Available online: https://www.kistler.com/files/document/000-710e.pdf?callee=frontend (accessed on 17 July 2021).
3. Zhao, Y.; Zhao, Y.L.; Shao, Y.W.; Hu, T.J.; Zhang, Q.; Ge, X.H. Research of a smart cutting tool based on MEMS strain gauge. *J. Phys. Conf. Ser.* **2018**, *986*, 012016. [CrossRef]
4. Yaldız, S.; Ünsaçar, F. Design, development and testing of a turning dynamometer for cutting force measurement. *Mater. Des.* **2006**, *27*, 839–846. [CrossRef]
5. Zhao, Y.; Wang, C.; Liang, S.; Cheng, R.; Qin, Y.; Wang, P.; Li, Y.; Li, X.; Hu, T. Design and development of a cutting force sensor based on semi-conductive strain gauge. *Sens. Actuators A Phys.* **2016**, *237*, 119–127. [CrossRef]
6. Zhang, Y.; Wu, W.; Han, Y.; Wen, H.; Cheng, Y.; Liu, L. Design and analysis of a turning dynamometer embedded in thin-film sensor. *Micromachines* **2019**, *10*, 210. [CrossRef]
7. Li, X.; Wu, W.; Cheng, Y.; Liu, L. Structure design and optimization for a cutting force measurement tool with embedded nickel-chromium film sensor. *Adv. Mech. Eng.* **2018**, *10*, 1–9. [CrossRef]
8. Rizal, M.; Ghani, J.A.; Husin, H.; Husaini, M.T. Design and construction a strain gauge-based dynamometer for a 3-axis cutting force measurement in turning process. *J. Mech. Eng. Sci.* **2018**, *4*, 4072–4087. [CrossRef]
9. Huang, J.; Pham, D.T.; Ji, C.; Zhou, Z. Smart cutting tool integrated with optical fiber sensors for cutting force measurement in turning. *IEEE Trans. Instrum. Meas.* **2020**, *69*, 1720–1727. [CrossRef]
10. Uquillas, D.A.R.; Yeh, S. Tool holder sensor design for measuring the cutting force in CNC turning machines. In Proceedings of the 2015 IEEE International Conference on Advanced Intelligent Mechatronics (AIM), Busan, Korea, 7–11 July 2015. [CrossRef]
11. Gong, T.; Zhao, Y.; Zhao, Y.; Wang, L.; Yang, Y.; Ren, W. Design and manufacturing of a high-sensitivity cutting force sensor based on AlSiCO ceramic. *Micromachines* **2021**, *12*, 63. [CrossRef] [PubMed]
12. Kim, J.H.; Chang, H.K.; Han, D.C.; Jang, D.Y. Cutting force estimation by measuring spindle displacement in milling process. *CIRP Ann. Manuf. Technol.* **2005**, *54*, 67–70. [CrossRef]
13. Xie, Z.; Lu, Y.; Li, J. Development and testing of an integrated smart tool holder for four-component cutting force measurement. *Mech. Syst. Signal Process.* **2017**, *93*, 225–240. [CrossRef]
14. Wang, C.; Rakowski, R.; Cheng, K. Design and analysis of a piezoelectric film embedded smart cutting tool. *Proc. Inst. Mech. Eng. Part B J. Eng. Manuf.* **2013**, *227*, 254–260. [CrossRef]
15. Chen, X.; Cheng, K.; Wang, C. Design of a smart turning tool with application to in-process cutting force measurement in ultra-precision and micro cutting. *Manuf. Lett.* **2014**, *2*, 112–117. [CrossRef]
16. Xiao, C.-W.; Cheng, K.; Ding, H.; Chen, S.-J. Design and analysis of a self-sensing smart cutting tool integrated piezoelectric films for cutting force monitoring in ultra-precision machining. In Proceedings of the 2013 Symposium on Piezoelectricity, Acoustic Waves, and Device Applications, Changsha, China, 25–27 October 2013. [CrossRef]
17. Nguyen, V.; Melkote, S.; Deshamudre, A.; Khanna, M.; Walker, D. PVDF sensor based monitoring of single-point cutting. *J. Manuf. Process.* **2016**, *24*, 328–337. [CrossRef]
18. Tschätsch, H. *Applied Machining Technology*; Springer: Berlin/Heidelberg, Germany, 2009; pp. 5–23. [CrossRef]
19. Black, S.C.; Chiles, V.; Lissaman, A.J.; Martin, S.J. *Principle of Engineering Manufacture*, 3rd ed.; Butterworth-Heinemann: New York, NY, USA, 2002; pp. 246–255, ISBN 0340631953.
20. Lai, Y. A Study of Aluminum Alloy 6061-T6 Turning with Different Characteristic of Unchamfered and Chamfered Main Cutting Edge Tools. Master's Thesis, Department of Mechanical and Electro-Mechanical Engineering, National ILan University, Yilan, Taiwan, 3 January 2020. [CrossRef]
21. Shotter, T. How to minimize warm-up drift in pressure sensors. In *Engineering Resources*; Leslie, G., Ed.; All Sensors Corp.: Morgan Hill, CA, USA, 2007. Available online: https://allsensors.com/engineering-resources/white-papers/warm-up-drift (accessed on 27 July 2021).
22. Lakić, G.G.; Kramar, D.; Kopač, J. *Metal Cutting—Theory and Applications*; University of Banja Luka: Banja Luka, Bosnia and Herzegovina, 2014; p. 77, ISBN 978-961-6536-85-1.
23. Altintas, Y. *Manufacturing Automation—Metal Cutting Mechanics, Machine Tool Vibrations, and CNC Design*, 2nd ed.; Cambridge University Press: New York, NY, USA, 2012; pp. 4–14, ISBN 978-1-107-00148-0.
24. Horváth, R. A new model for fine turning forces. *Acta Ploytechnica Hung.* **2015**, *12*, 109–128. [CrossRef]